^{1}H and ^{13}C NMR Studies of an Oxidized HiPIP

Ivano Bertini,*,† Antonio Donaire,† Isabella C. Felli,† Claudio Luchinat,‡ and Antonio Rosato†

Departments of Chemistry and of Soil Science and Plant Nutrition, University of Florence, Florence, Italy

Received January 17, 1997[⊗]

^{1}H−^{13}C HETCOR NMR spectra have been recorded for the oxidized HiPIP I from *Ectothiorhodospira halophila* for which an extended ^{1}H assignment was available. The hyperfine shifts of the α and β carbons of the coordinated cysteines, as well as those of their attached protons, have been discussed in terms of the current magnetic coupling models and of the mechanisms of spin density delocalization. Through HSQC spectra preceded by a proton 180° pulse, the nonselective T_1 values of the protons have been accurately obtained. It is shown how the nuclear T_1 values can be used as constraints, together with NOEs, for solution structure determination even when the present magnetic coupling scheme occurs. The oxidized cluster is shown to have an effective relaxation time much shorter than that in the reduced state.

Introduction

High-potential iron−sulfur proteins (HiPIPs) are a class of small proteins containing an Fe_4S_4 cluster. The biologically relevant oxidation states of the cluster are 3+ and 2+. The biological function of HiPIPs is not well understood, although it is likely that they are involved in the electron transfer process of the photosynthetic center in photosynthetic bacteria.[1]

In the oxidized species, the polymetallic center formally contains three Fe^{3+} ions and one Fe^{2+} ion, and in the reduced species, it contains two Fe^{3+} ions and two Fe^{2+} ions. Actually, in the latter species, all iron ions are in the 2.5+ oxidation state,[2,3] whereas in the oxidized species, two iron pairs can be distinguished: a ferric pair, containing two Fe^{3+} ions, and a mixed-valence pair, containing two $Fe^{2.5+}$ ions.[3−5]

Each pair could in principle be localized on any of the edges of the Fe_4 tetrahedron. However, the electrostatic potential due to protein and solvent atoms around the cluster makes the different valence distributions nonequivalent, and indeed only two such distributions are experimentally observed.[6] The equilibrium between the two species is fast on the NMR time scale, and it has been proposed[4] that they can be detected only through EPR measurements at low temperature.

In the case of HiPIP I from *Ectothiorhodospira halophila*, the molar ratios of the two species are 0.8 and 0.2. The charges are distributed as follows: Cys33-Fe^{3+} (100%), Cys36-$Fe^{2.5+}$ (80%), Cys50-$Fe^{2.5+}$ (100%), Cys66-Fe^{3+} (80%).[7] The charge distribution is depicted in Figure 1.

HiPIPs are the first paramagnetic proteins for which a thorough NMR investigation has led to the determination of the solution structure in both the oxidized and the reduced state.[8−11] Recently the present HiPIP, labeled with ^{13}C and ^{15}N, was investigated in the reduced state with the use of heteronuclear NMR techniques.[12] A quite extensive assignment of proton and heteronuclear resonances was obtained. The Fe−S−Cβ−Cα dihedral angles were estimated from the hyperfine shifts of the β protons and of the α carbon. Finally, proton nuclear relaxation rates were measured and used as structural constraints for solution structure determination.[12]

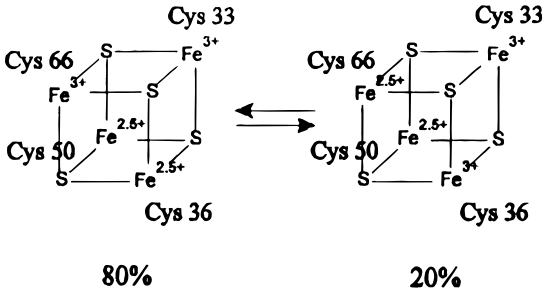

Figure 1. Distribution of the charges in the cluster of the oxidized HiPIP I from *E. halophila* with the equilibrium proposed on the basis of the hyperfine shifts of the βCH_2 protons of the coordinated cysteines (from ref 7).

In the present paper, an investigation of the cysteine ^{13}C nuclei in the oxidized form is reported, which led to an almost complete assignment of the cysteine resonances. Comparison of the ^{13}C shifts with the proton shifts and the shifts of the reduced species is instructive for understanding the subtleties of unpaired spin density delocalization mechanisms. The pairwise separation of valencies introduces large anisotropy, besides the already known anisotropy in the shifts, in nuclear relaxation properties as already observed for an analogous system.[13] The anisotropy

* Corresponding author. Phone: 39 55 2757549. Fax: 39 55 2757555. E-mail: bertini@risc1.lrm.fi.cnr.it.
† Department of Chemistry.
‡ Department of Soil Science and Plant Nutrition.
⊗ Abstract published in *Advance ACS Abstracts,* September 1, 1997.

(1) Hochkoeppler, A.; Ciurli, S.; Venturoli, G.; Zannoni, D. *FEBS Lett.* **1995**, *357*, 70−74.
(2) Dickson, D. P. E.; Johnson, C. E.; Cammack, R.; Evans, M. C. W.; Hall, D. O.; Rao, K. K. *Biochem. J.* **1974**, *139*, 105.
(3) Middleton, P.; Dickson, D. P. E.; Johnson, C. E.; Rush, J. D. *Eur. J. Biochem.* **1980**, *104*, 289−296.
(4) Bertini, I.; Campos, A. P.; Luchinat, C.; Teixeira, M. *J. Inorg. Biochem.* **1993**, *52*, 227−234.
(5) Bertini, I.; Ciurli, S.; Luchinat, C. *Struct. Bonding* **1995**, *83*, 1−54.
(6) Banci, L.; Bertini, I.; Ciurli, S.; Ferretti, S.; Luchinat, C.; Piccioli, M. *Biochemistry* **1993**, *32*, 9387−9397.
(7) Bertini, I.; Capozzi, F.; Eltis, L. D.; Felli, I. C.; Luchinat, C.; Piccioli, M. *Inorg. Chem.* **1995**, *34*, 2516−2523.
(8) Banci, L.; Bertini, I.; Eltis, L. D.; Felli, I. C.; Kastrau, D. H. W.; Luchinat, C.; Piccioli, M.; Pierattelli, R.; Smith, M. *Eur. J. Biochem.* **1994**, *225*, 715−725.
(9) Bertini, I.; Eltis, L. D.; Felli, I. C.; Kastrau, D. H. W.; Luchinat, C.; Piccioli, M. *Chem.—Eur. J.* **1995**, *1*, 598−607.
(10) Banci, L.; Bertini, I.; Dikiy, A.; Kastrau, D. H. W.; Luchinat, C.; Sompornpisut, P. *Biochemistry* **1995**, *34*, 206−219.
(11) Bertini, I.; Dikiy, A.; Kastrau, D. H. W.; Luchinat, C.; Sompornpisut, P. *Biochemistry* **1995**, *34*, 9851−9858.
(12) Bertini, I.; Couture, M. M. J.; Donaire, A.; Eltis, L. D.; Felli, I. C.; Luchinat, C.; Piccioli, M.; Rosato, A. *Eur. J. Biochem.* **1996**, *241*, 440−452.
(13) Huber, J. G.; Moulis, J.-M.; Gaillard, J. *Biochemistry* **1996**, *35*, 12705−12711.

S0020-1669(97)00057-8 CCC: $14.00

in relaxation and shifts has been related to the electronic structure of the polymetallic center. This advancement in the knowledge of the system has made nuclear relaxation exploitable for the determination of solution structures of this type of proteins. A procedure is proposed here which is different from that used in the case of the reduced protein,[12] which contains only $Fe^{2.5+}$ ions.

Experimental Section

^{13}C,^{15}N-labeled HiPIP I from *E. halophila* was obtained as previously described.[12] Two samples, in H_2O and in D_2O, were oxidized with a 10 mM $[Fe(CN)_6]^{3-}$ solution. Excess oxidant was eliminated by exchanging the sample several times against a 50 mM phosphate buffer solution (pH = 5.2) by ultrafiltration (Amicon, YM3 membranes). The final concentrations of the samples were around 2 mM.

All NMR experiments were performed on a Bruker AMX 600 spectrometer or on a Bruker DRX 500 spectrometer. The temperature was typically set up to 288 K, unless otherwise specified. Data were processed with the standard Bruker software and analyzed with the program XEASY[14] on IBM RISC 6000/530 computers.

For the heteronuclear assignments, ^{13}C and ^{15}N HSQC,[15] HNCA,[16] and HNCOCA[17] experiments were performed. For the HNCA and HNCOCA experiments, only Cα evolution was allowed. The parameters used in these experiments are those previously published for the reduced form.[12] A constant-time HCCH experiment[18] in the 2D version mode with the ^{1}H and ^{13}C carriers shifted on the aromatic region was also performed in order to relate aromatic protons to carbons of the same ring not directly bound to them.

For the assignment of the hyperfine nuclei of the coordinated cysteines, ^{13}C HSQC experiments were performed with the transfer delays shortened to 800 ms, with spectral windows of 300 and 100 ppm for the ^{13}C and ^{1}H dimensions, respectively, and with the carrier shifted at different positions of the spectrum according to the chemical shift of the observed signal (from 40 to 400 ppm for the ^{13}C nucleus and from 4.93 to 45 ppm for protons).

Nonselective relaxation times of unresolved protons were obtained from inversion-recovery HSQC experiments.[12] Ten experiments with delay times ranging from 1 to 1000 ms were performed for amide protons using an H_2O protein sample and for aromatic and aliphatic protons using a D_2O protein sample. The obtained intensities were fitted as a function the recovery delay, *t*, through a three-parameter monoexponential equation of the type[19]

$$\langle I(t)\rangle = \langle I(\infty)\rangle - (\langle I(\infty)\rangle - \langle I(0)\rangle)\exp(-\rho_I^{\text{eff}} t) \qquad (1)$$

The paramagnetic contributions to the ρ_I^{eff} parameters were obtained by subtracting average diamagnetic contributions of 3.5 and 1.3 s^{-1} for the amide and for the aliphatic protons, respectively. These values gave the best correlation between calculated (ρ_I^{calc}) and experimental (ρ_I^{para}) paramagnetic contributions to nuclear relaxation rates and are close to previously obtained ones.[12,13,19]

NOE constraints were converted into upper distance limits through the program CALIBA, by following the standard methodology.[20] Structure calculations were performed with the program DYANA.[21] A total of 100 random structures were generated and annealed in 12 000 steps, and the 20 best structures (in terms of total target function) were included in the final family of structures. The same calculation was repeated with and without inclusion of ρ_I^{para} constraints.

All calculations were run on IBM RISC6000 computers.

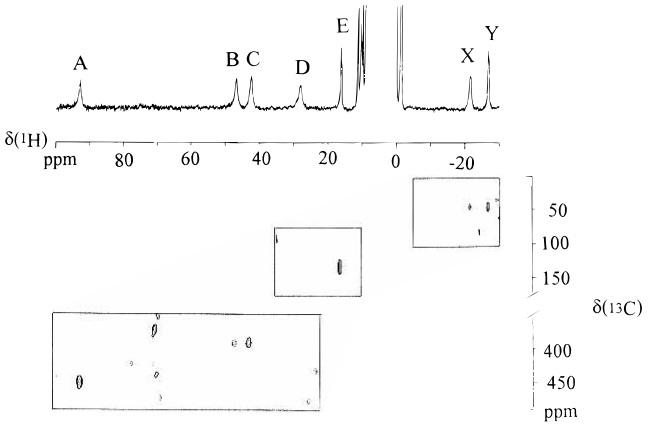

Figure 2. Top: 600 MHz 1D spectrum of recombinant oxidized HiPIP I from *E. halophila* (A, Cys 50 Hβ2; B, Cys 36 Hβ1; C, Cys 36 Hβ2; D, Cys 50 Hβ1; E, Cys 66 Hα; X, Cys 33 Hβ1; Y, Cys 33 Hβ2). Bottom: various portions of HSQC spectra showing the ^{1}H-^{13}C connectivities used to assign the hyperfine shifted cysteine carbons.

Results and Discussion

^{1}H and ^{13}C Chemical Shifts. The different electronic properties of the two iron pairs in the $[Fe_4S_4]^{3+}$ cluster cause dramatic differences in the hyperfine shifts of ^{13}C and ^{1}H nuclei of the cysteines coordinating to the polymetallic center. Figure 2 shows the 1D spectrum of oxidized recombinant HiPIP I from *E. halophila* at 288 K, together with portions of the various ^{1}H−^{13}C HSQC spectra tailored to detect ^{1}H−^{13}C connectivities among hyperfine-shifted, fast-relaxing signals. The chemical shift data relative to the α and the β carbons, and the α and β protons are reported in Table 1, together with the the chemical shifts observed for the reduced species.[12] It is interesting to note that the ^{13}C dispersion for cysteine β carbons is roughly 400 ppm.

In the reduced state, the hyperfine shifts of the above signals all have the same sign, as the measured chemical shifts are all downfield with respect to the average diamagnetic values. Moreover, the shifts of the β carbons are similar for the four cysteines, thus confirming the hypothesis that the electron properties of the four iron ions in the reduced state are similar to each other.[22−24] In the case of β protons and α carbons, the dependence of the hyperfine shift on the Fe−Cβ−S−nucleus dihedral angle[25] largely contributes to the differences in the observed hyperfine shifts among the four cysteines. The above considerations may be extended to all $[Fe_4S_4]^{2+}$ clusters, either in HiPIPs or in ferredoxins. From the data available in the literature regarding oxidized low-potential ferredoxins, it is apparent that both the magnitude and the pattern of proton[25−28] and carbon[25,26] chemical shifts are very similar to those observed for HiPIP I from *E. halophila* in the reduced state. It is thus reasonable to assume that the delocalization of unpaired electron

(14) Eccles, C.; Güntert, P.; Billeter, M.; Wüthrich, K. *J. Biomol. NMR* **1991**, *1*, 111−130.
(15) Bodenhausen, G.; Ruben, D. J. *Chem. Phys. Lett.* **1980**, *69*, 1985.
(16) Kay, L. E.; Ikura, M.; Tschudin, R.; Bax, A. *J. Magn. Reson.* **1990**, *89*, 496−514.
(17) Bax, A.; Ikura, M. *J. Biomol. NMR* **1991**, *1*, 99−104.
(18) Clore, G. M.; Bax, A.; Driscoll, P. C.; Wingfield, P. T.; Gronenborn, A. M. *Biochemistry* **1990**, *29*, 8172−8184.
(19) Bertini, I.; Donaire, A.; Luchinat, C.; Rosato, A. *Proteins: Struct., Funct., Genet.*, in press.
(20) Güntert, P.; Braun, W.; Wüthrich, K. *J. Mol. Biol.* **1991**, *217*, 517−530.
(21) Güntert, P.; Mumenthaler, C.; Wüthrich, K. Submitted for publication.
(22) Noodleman, L. *Inorg. Chem.* **1988**, *27*, 3677−32679.
(23) Blondin, G.; Girerd, J.-J. *Chem. Rev.* **1990**, *90*, 1359−1376.
(24) Banci, L.; Bertini, I.; Briganti, F.; Luchinat, C.; Scozzafava, A.; Oliver, M. V. *Inorg. Chem.* **1991**, *30*, 4517−4524.
(25) Bertini, I.; Capozzi, F.; Luchinat, C.; Piccioli, M.; Vila, A. J. *J. Am. Chem. Soc.* **1994**, *116*, 651−660.
(26) Scrofani, S. D. B.; Brownlee, R. T. C.; Sadek, M.; Wedd, A. G. *Inorg. Chem.* **1995**, *34*, 3942−3952.
(27) Wildegger, G.; Bentrop, D.; Ejchart, A.; Alber, M.; Hage, A.; Sterner, R.; Roesch, P. *Eur. J. Biochem.* **1995**, *229*, 658−668.
(28) Donaire, A.; Zhou, Z.-H.; Adams, M. W. W.; La Mar, G. N. *J. Biomol. NMR* **1996**, *7*, 35−47.

Table 1. Chemical Shifts of the ^{13}C and ^{1}H Nuclei in the Coordinated Cysteines of HiPIP I from *E. halophila* in the Reduced[12]and Oxidized Species (Present Work)[a]

	ppm				dihedral angle	
	reduced		oxidized			
nucleus	288 K	283 K	288 K	298 K	atoms	value (deg)
			Cys 33 (Fe^{3+} 100%)			
Cβ	102.3	35.8	41.1			
Hβ1	7.5	−22.8	−21.58	−16.3	Fe−S−Cβ−Hβ1	175.3
Hβ2	16.5	−27.4	−26.7	−24.1	Fe−S−Cβ− Hβ2	57.5
Cα	86.7		54.7		Fe−S−Cβ−Cα	−63.6
Hα						
			Cys 36 ($Fe^{2.5+}$ 80%)			
Cβ	103.7	394.9	390			
Hβ1	9.06	47.1	47.0	45.2	Fe−S−Cβ−Hβ1	75.4
Hβ2	7.5	42.6	42.4	41.1	Fe−S−Cβ− Hβ2	−42.2
Cα	78.2		28.6		Fe−S−Cβ−Cα	−163.4
Hα	3.81		0.62			
			Cys 50 ($Fe^{2.5+}$ 100%)			
Cβ	112.4	450	440			
Hβ1	4.7	28.2	27.8	27.0	Fe−S−Cβ−Hβ1	−18.4
Hβ2	14.3	94.0	92.0	88.1	Fe−S−Cβ− Hβ2	−136.5
Cα	89.0		153.2		Fe−S−Cβ−Cα	102.5
Hα	4.16		6.48			
			Cys 66 (Fe^{3+} 80%)			
Cβ	88.7		59.3			
Hβ1	10.8		6.26	8.3	Fe−S−Cβ−Hβ1	138.0
Hβ2	5.81		2.59	4.1	Fe−S−Cβ−Hβ2	20.5
Cα	85.8	126.7	129.0		Fe−S−Cβ−Cα	−100.7
Hα	7.74	15.9	16.2			

[a] The reference diamagnetic chemical shifts are as follows:[25,44] Cβ 31 ppm, Hβ 2.8 ppm, Cα 60 ppm, Hα 4.2 ppm. It should be noted that the most extensive assignments for the oxidized form are reported at 288 K, as the complete set of tailored experiments described in the Experimental Section (such as 1D NOEs,[7] HNCA, HNCACO, etc.) was acquired only at this temperature. Only part of these experiments were repeated at the other two temperatures, yielding partial, but meaningful, assignments.

spin density over the cysteine atoms is affected to a negligible extent by the different protein environments around the polymetallic center. It is also likely that the properties of the oxidized $[Fe_4S_4]^{3+}$ cluster of HiPIP I from *E. halophila*, which will be discussed below, are general for all $[Fe_4S_4]^{3+}$ clusters occurring in the various HiPIPs.

For the oxidized species, the pattern of chemical shifts changes dramatically with respect to that for the reduced species. The β carbon resonances of cysteines 36 and 50 are shifted far downfield (the observed chemical shifts at 288 K are 390 and 440 ppm, respectively), whereas in the case of cysteines 33 and 66, only slight hyperfine shifts are observed (the chemical shifts at 288 K are 41.1 and 59.3 ppm, respectively). The former two cysteines coordinate mainly to the mixed-valence pair, and the latter two coordinate mainly to the ferric pair. As far as the β protons are concerned, those of cysteines 36 and 50 sense a sizable hyperfine shift, downfield with respect to the diamagnetic region (see Table 1). The β protons of cysteine 33 are well shifted in the upfield region of the spectrum, whereas the β protons of cysteine 66 are hidden under the diamagnetic envelope. The differences in the magnitudes of the hyperfine shifts of the two β protons within each cysteine may be related to their dependence on the Fe−Cβ−S−nucleus dihedral angle, as already noted for the reduced species (see above). The pattern of chemical shifts of the α carbons appears more complicated, as in the ferric pair the α carbon of cysteine 33 is shifted in the upfield region of the spectrum, whereas that of cysteine 66 is shifted in the downfield region. In the mixed-valence pair, the α carbon of cysteine 36 is upfield-shifted, whereas that of cysteine 50 is downfield-shifted.

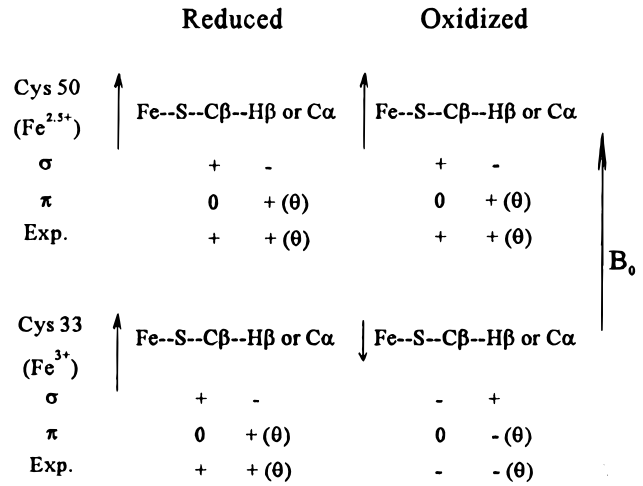

Figure 3. Representation of the σ and π contributions to the hyperfine shifts for an iron ion belonging to the mixed-valence pair (cysteine 50) and to the ferric pair (cysteine 33) in both reduced and oxidized states. A symbol within parentheses is indicative of a large expected Fe−S−C−Bβ−Cα dihedral angle dependence.

Two mechanisms have been postulated to be operative for spin delocalization in aliphatic systems and, thus, for the hyperfine shift.[25] The first will be referred to as direct spin density transfer, the intensity of which attenuates with increasing number of bonds, and the second is spin polarization, which is particularly effective between two orthogonal orbitals, one of which contains one electron and the other two electrons. The first mechanism gives rise to spin density of the same sign as that sensed by the nucleus of the donor atom (positive spin density), while the second provides spin density of the opposite sign on neighbor nuclei. The direct mechanism also has a dependence on the conformation of the molecule. As will be discussed later, geometric factors play an important role in determining the relative weight of the two contributions.

In order to understand the mechanisms responsible for the delocalization of the unpaired electron spin density on the cysteine atoms, it is convenient to compare the shift patterns observed in the reduced and oxidized states. First, let us focus on the hyperfine shifts of the β carbons. In the reduced species, all four β carbons are downfield-shifted (Table 1). This is due to the direct delocalization of unpaired electron spin density on the nucleus (Figure 3). In the oxidized species, the β carbons of cysteines 36 and 50 are downfield-shifted. This is not unexpected, as in the oxidized $[Fe_4S_4]^{3+}$ cluster, the individual electron spins in the mixed-valence pair are oriented along the magnetic field, just as in the reduced species. Therefore, we can conclude that the sign of the electron−nucleus coupling for the nuclei of the cysteines coordinating to the mixed-valence pair is the same in the reduced and oxidized species. The sign should be reversed for the nuclei of the cysteines coordinating to the ferric pair, as the individual electron spins in the pair are aligned along the magnetic field in the reduced state and against the field in the oxidized state. For the β carbons of cysteines 33 and 66, coordinated to the ferric pair, the observed hyperfine shift at 288 K is small and downfield. According to the above reasoning, they would be expected to be upfield-shifted. However, the temperature dependence of the β carbon shift of cysteine 33 is very strong (nearly 5 ppm over 5 K; see Table 1), and the resonance moves toward the upfield region of the spectrum as the temperature decreases. This shows that the electron density distribution in the ground state is that predicted and that population of excited states accounts for the slight downfield shifts. The larger hyperfine shifts observed for the β carbons of cysteines 36 and 50, coordinated to the mixed-

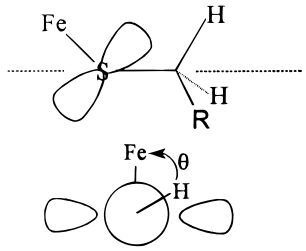

Figure 4. Schematic view of the Fe−S−Cβ−Hβ dihedral angle for the metal−donor−CH_2 moiety. A sulfur p_z orbital orthogonal to the Fe−S−Cβ plane is also shown.

valence pair, in the oxidized species with respect to the reduced one are due to the increased overall paramagnetism of the cluster.

The β protons in the reduced species are again all hyperfine shifted in the downfield region of the spectrum (Table 1). Again, this shows that positive unpaired electron spin density is present at the proton. The magnitude of the hyperfine shifts in the reduced species varies from more than 13 ppm (Hβ2 of cysteine 33) to ca. 2 ppm (Hβ1 of cysteine 50). This finding has been explained by assuming that the magnitude of the shift is determined essentially by the overlap of the proton *s* orbital with the p_z orbital of the sulfur, which depends on the sine squared of the Fe−S−Cβ−Hβ (θ) dihedral angle (Figure 4)[25]. The hyperfine shift is thus expected to be larger when the angle is close to ±90° and smaller when it is close to 0 or 180°. Indeed, this is experimentally confirmed (see Table 1).

The same principles allow the interpretation of the hyperfine shifts observed for the oxidized species. The β proton signals of the cysteines coordinating to the mixed-valence pair are hyperfine shifted at 288 K in the downfield region of the spectrum (Table 1), as expected. The differences in the shifts measured can be accounted for on the basis of: (1) the dihedral angle dependence described above and (2) the equilibrium between different charge distributions[7] (see previous section and Figure 1). Concerning the ferric pair, at 288 K the β protons of cysteine 33 are upfield-shifted as expected, whereas those of cysteine 66 are slightly downfield-shifted. This difference is likely to be due to the equilibrium between different charge distributions.[7] However, in both cases, a strong temperature dependence is observed: as in the case of the corresponding β carbons, the hyperfine shift is observed to become negative, as expected, with decreasing temperature.

In the reduced species, all α carbons are hyperfine shifted in the downfield region of the spectrum at 288 K (Table 1). This is indicative of the fact that the same electron delocalization mechanisms are operative for β protons and α carbons. In the oxidized species, at 288 K the ferric pair shows an α carbon with very small hyperfine shift (cysteine 33) and an α carbon downfield-shifted (cysteine 66). The temperature dependence of the latter is such that the hyperfine shifts quickly decrease with decreasing temperature. This is strictly analogous to the behavior observed for the β protons. In the case of the mixed-valence pair, the α carbon of cysteine 50 is sizably downfield-shifted, as expected, whereas that of cysteine 36 is surprisingly upfield-shifted (a slight upfield shift is also observed for its Hα proton). A possible explanation for this behavior could stem from the value of the Fe−S−Cβ−Cα dihedral angle that is closer to 180° for Cys 36 and closer to 90° for Cys 50 (Table 1). In the case of Cys 50, the overall positive spin density could be due to the dominance of the direct spin density transfer from the sulfur p orbital, while in the case of Cys 36, this contribution is much smaller and spin-polarization effects, though small, may prevail.

In summary, all hyperfine shift data in Table 1 for both the oxidized and the reduced species could be rationalized in terms of electron delocalization mechanisms that are plausible and consistent with all the previous knowledge of this class of proteins. In particular, the picture is consistent with the different electronic distributions within the two oxidation states arising from different manifestations of the so-called spin frustration. Indeed, in the reduced $[Fe_4S_4]^{2+}$ cluster, characterized by an $S = 0$ ground state, the fractional unpaired spin densities on each of the four iron ions (due to low-lying paramagnetic excited states) are nearly equivalent and, in particular, have all the same sign. In the oxidized $[Fe_4S_4]^{3+}$ cluster, having an $S = {}^1/_2$ ground state, only the electron spin populations in the mixed-valence pair are aligned along the external magnetic field, whereas spin frustration forces the electron spin populations in the ferric pair to be oriented *against* the magnetic field. As has been shown, taking this effect into account is essential for a correct understanding of the actual electron delocalization mechanisms on the nuclei in the oxidized species. Furthermore, the value of the Fe−S−Cβ−Hβ(Cα) torsion angle plays an important role in this σ type electron delocalization mechanism.

The Nuclear Relaxation Rates. The measurement of proton nuclear relaxation rates provides further insights into the different electron properties of the two iron pairs. Indeed, their analysis may provide an estimate of the ratio of electron magnetic moments in the two pairs under the assumption that the electronic relaxation rates are the same for all four iron ions in the cluster.[29] An analysis of nuclear relaxation properties in a similar system recently appeared in the literature.[13] We here take the opportunity to rediscuss the theoretical aspects of the electronic structure of this type of clusters.

The contribution to the nuclear longitudinal relaxation rates due to the unpaired electron spin density present on the iron ions essentially arises from the metal-centered dipolar interaction between the electron spin and the nuclear spin. Indeed, Curie effects[30,31] on nuclear longitudinal relaxation rates in macromolecules are negligible,[32] whereas contact[33,34] and ligand-centered dipolar relaxation rapidly fall off as the number of σ bonds between the metal ion and the resonating nucleus increases and, in practice, might be relevant only for the β protons of the cysteines coordinating the iron ions.[35] Thus, the nuclear relaxation rates of such protons were only included as a verification at the end of the analysis.

Electron−nucleus dipolar interaction is described by the Solomon equation[36]

$$R_{1J}^{(I)} = \frac{2}{15}\left(\frac{\mu_0}{4\pi}\right)^2 \frac{\gamma_I^{\,2} g_e^{\,2} \mu_B^{\,2} S(S+1)}{r_{IJ}^{\,6}}\left(\frac{7\tau_S}{1+\omega_S^{\,2}\tau_S^{\,2}} + \frac{3\tau_S}{1+\omega_I^{\,2}\tau_S^{\,2}}\right) \quad (2)$$

where γ_I is the nuclear magnetogyric ratio g_e is the electronic *g* factor, μ_B is the electron Bohr magneton, *S* is the electron spin angular momentum, r_{IJ} is the distance from the metal *J* to proton *I*, τ_S is the electronic relaxation time, ω_I and ω_S are the Larmor frequencies of the proton and the electron, respectively, and all

(29) Bertini, I.; Galas, O.; Luchinat, C.; Parigi, G.; Spina, G. Submitted for publication.
(30) Vega, A. J.; Fiat, D. *Mol. Phys.* **1976**, *31*, 347−362.
(31) Gueron, M. J. *Magn. Reson.* **1975**, *19*, 58−66.
(32) Bertini, I.; Luchinat, C. *NMR of paramagnetic molecules in biological systems*; Benjamin/Cummings: Menlo Park, CA, 1986.
(33) Solomon, I.; Bloembergen, N. *J. Chem. Phys.* **1956**, *25*, 261−266.
(34) Bloembergen, N. *J. Chem. Phys.* **1957**, *27*, 572−573.
(35) Ciurli, S.; Cremonini, M. A.; Kofod, P.; Luchinat, C. *Eur. J. Biochem.* **1996**, *236*, 405−411.
(36) Solomon, I. *Phys. Rev.* **1955**, *99*, 559−565.

other symbols have their usual meaning. For the sake of simplicity, eq 2 for nucleus I interacting with metal J can be rewritten as

$$R_{1J}^{(I)} = K_J r_{IJ}^{-6} \quad (3)$$

where all the electronic parameters, as well as all the constants, have been collected in K_J.

In a metal-centered approximation, the overall contribution of the unpaired spin density present on the polymetallic center to the nuclear relaxation rates is given by

$$R_1^{(I)} = \sum_{J=1}^{4} K_J r_{IJ}^{-6} \quad (4)$$

where the sum is extended to the four metal ions. The fact that two species exist in solution (with an 80/20 ratio) differing because of their valence distribution[7] (Figure 1) must also be taken into account. To do this, eq 4 has to be modified to

$$R_1^{(I)} = K_1 r_{I1}^{-6} + (0.8K_2 + 0.2K_4) r_{I2}^{-6} + K_3 r_{I3}^{-6} + (0.2K_2 + 0.8K_4) r_{I4}^{-6} \quad (5)$$

where 1 labels the iron ion bound to Cys 33 (whose charge is 3+), 2 the iron ion bound to Cys 36 (mainly 2.5+), 3 the iron ion bound to Cys 50 (2.5+), and 4 the iron ion bound to Cys 66 (mainly 3+).

The effective paramagnetic contributions to the nuclear relaxation rates (ρ_I^{para}) were obtained from the proton longitudinal relaxation rates by subtracting average diamagnetic contributions of 3.5 and 1.3 s^{-1} for the amide and for all other protons, respectively (see the Experimental Section). The ρ_I^{para} values were then used as structural constraints through eq 5, with the simplification that the iron ions in each pair were assumed to have the same K_J value ($K_1 = K_4$; $K_2 = K_3$). In this way, only two different parameters are needed. In the case of the reduced species, only one K was needed in eq 5, as in the reduced cluster all iron ions are equivalent.[2,3] In our previous studies,[12,19,37] only proton−metal upper distance limits were used in calculations, and thus only an upper limit for K was estimated. In the present case, the procedure is more complicated because there are two K values to be determined. Therefore, the solution structure obtained from NOEs[9] was used as the input structure to obtain the K values from the experimental ρ^{para} values. Then the metal to proton distances were back-calculated, and the solution structure was solved again by imposing as constraints NOEs and ρ_I^{para} simultaneously. The NOE intensities were transformed into proton−proton upper distance limits through the program CALIBA.[20] A total of 1125 meaningful upper distance limits were obtained. A NOE is violated when the actual distance in the structural model is larger than the estimated upper distance limit. ρ_I^{para} values were used to extract proton−metal distances, which were then allowed a ±15% tolerance. All protons with $T_1 < 150$ ms were used in calculations, except for cysteine β protons and for all nonstereospecifically assigned geminal protons. A total of 27 constraints were used in the calculations. After DYANA calculations, a family of 20 structures was obtained which is consistent with both sets of structural constraints. The average contribution to the target function of NOEs and van der Waals violations per structure rose from 0.31 ± 0.10 to 0.53 ± 0.14 Å^2 upon inclusion of ρ^{para} derived constraints. The contribution of the latter to the target function is in the 0.01−0.1 Å^2 range. The total backbone pairwise RMSD is 0.62 ± 0.09 Å, which compares to the value of 0.63 ± 0.10 Å obtained with NOEs alone. The definiton of the two families obtained with and without ρ_I^{para} derived constraints is essentially the same. This is due to the fact that the numer of ρ_I^{para} constraints is small with respect to that of the NOEs. This, in turn, is due to the small relaxing capability of the system (see later). However, the ρ_I^{para} constraints, as included in calculations according to the procedure described in this paper, are reliable constraints, fully consistent with NOEs. These constraints give further confidence in the obtained protein structure. Furthermore, the ρ_I^{para} constraints provide direct structural information on the location of the metal ions in the protein frame. The definition of the polymetallic center itself is therefore dramatically improved upon introduction of these constraints, as can be seen from Figure 5. The relative impact of the NOEs and ρ_I^{para} constraints on the resolution of the protein structure depends mainly on the number of constraints of each type. It is expected that, in systems where a smaller number of NOEs is observed, the ρ_I^{para} constraints may be very important.

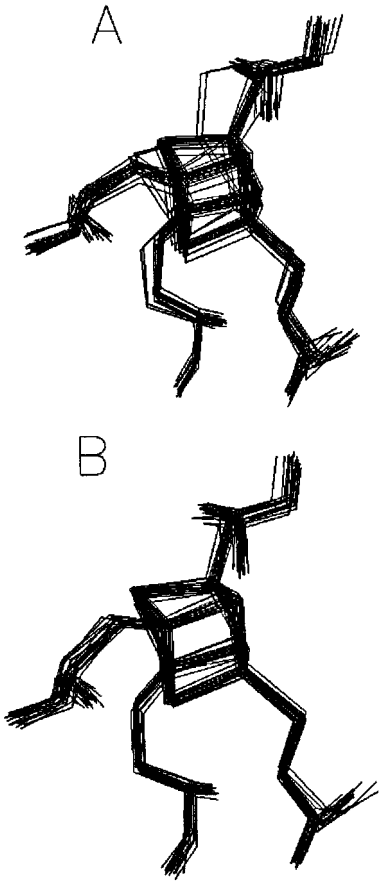

Figure 5. Close-ups of the polymetallic center in the DYANA families obtained without (A) and with (B) the use of the ρ_I^{para} constraints.

At the end of the procedure described above, the values of $K_1 = K_4 = 60\,000$ and $K_2 = K_3 = 200\,000$ s^{-1} Å^6 are obtained. Figure 6 shows the correlation between the ρ_I^{para} values and the distances taken from the solution structure. The data relative to β protons of the cysteine residues are added to the plot, although they were not used as structural constraints. The above values of K_1 and K_2 indicate that the nuclear relaxation pathway provided by the ferric pair is more than 3 times less efficient than that of the mixed-valence pair. This is consistent with the earlier observation that the relaxation rates of the β protons of the cysteines coordinating to the mixed-valence pair are sizably higher than those of the β protons of the cysteines coordinating

(37) Bertini, I.; Luchinat, C.; Rosato, A. *Prog. Biophys. Mol. Biol.* **1996**, *66*, 43−80.

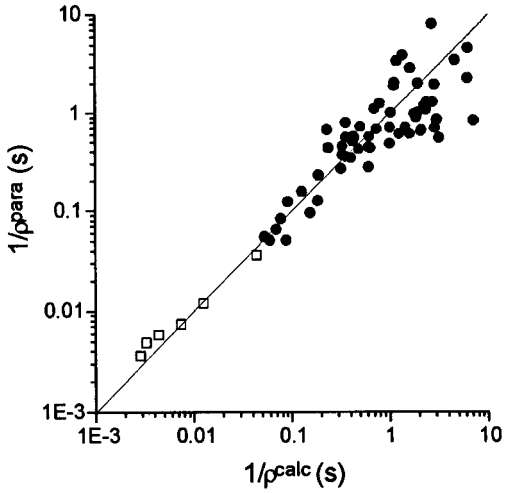

Figure 6. Plot of the experimental $1/(\rho^{para})$ versus the calculated $1/(\rho^{calc})$ relaxation rates according to eq 5 with $K_1 = 200\,000$ Å^6 s^{-1} and $K_2 = 60\,000$ Å^6 s^{-1}. Cysteine β protons (open squares) were not used for the fitting. The relaxation rates of the protons of cysteine 66 could not be measured because their signals were hidden under the diamagnetic envelope.

to the ferric pair.[7,9,13] The different values of K_J estimated for the two pairs can be explained in terms of the different contributions of each pair of iron ions to the populated energy levels. Indeed, such contributions are proportional to the individual magnetic moments of the iron ions,[38] and it is thus expected that the squared ratio of the populations of the two pairs is equal to the ratio of the K_J's, as defined in this work. Indeed, if calculations are performed on the basis of the Heisenberg exchange model, values close to the experimental ones are obtained. Essentially two models are available.[22,39] According to one model,[22] the ground state wave function contains a subspin of $^9/_2$ for the mixed-valence pair, and a subspin of 4 for the ferric pair. In the other model,[39] the ground state wave function is a linear combination of the above state and of another state where the subspin of the mixed-valence pair is $^7/_2$ and that of the ferric pair is still 4. Despite the fact that the latter model better explains the experimental hyperfine coupling constants determined through Mössbauer spectroscopy,[4] both models account equally well for the observed difference between the two iron pairs with respect to the enhancement of nuclear relaxation rates.

The value of the K_2 constant found for the iron ions of the mixed-valence pair (200 000 Å^6 s^{-1}) is the same as that found for the four equivalent iron ions in the reduced species,[40] while the value of K_1 found for the ferric pair is sizably smaller (60 000 Å^6 s^{-1}). This is in agreement with the smaller nuclear relaxation rate enhancements observed for the nuclei in the neighborhoods of the ferric pair in the oxidized state. Anyhow, the larger hyperfine shifts observed for the mixed-valence pair in the oxidized form and the larger overall magnetic moment of the oxidized cluster ($\mu_{eff} = 1.8\ \mu_B$, vs $\mu_{eff} = 0.8\ \mu_B$ for the reduced species), together with theoretical calculations, suggest that the individual magnetic moments on each iron atom are larger in the oxidized than in the reduced form. Since the unpaired electron in the cluster has only one effective relaxation time, a reduction of such time in the oxidized species is the only possible explanation to account for the smaller nuclear relaxation rate enhancements induced by the oxidized cluster.

Conclusions

The present investigation provided a thorough assignment of ^{1}H and ^{13}C resonances of the cysteines coordinating to the polymetallic center in the oxidized HiPIP I from *E. halophila*, which complements that already available for the reduced species.[12] Deeper insights into the electron delocalization mechanisms were obtained through a detailed comparison of the nuclear hyperfine shifts of the oxidized and reduced species.

The analysis of the nuclear relaxation enhancements due to electron−nucleus dipolar interaction led to a better understanding of the electronic structure in the oxidized $[Fe_4S_4]^{3+}$ cluster. It should be pointed out that, due to the fact that the protein was fully labeled in ^{13}C, it was possible to measure nuclear T_1's through inversion-recovery HSQC experiments. These experiments have higher sensitivity than homonuclear inversion-recovery experiments (e.g., IR-TOCSY, IR-NOESY, etc.) and provide more reliable measurements of nuclear T_1's.

Nuclear relaxation enhancements due to the paramagnetic center[12,19] and hyperfine shifts[41−43] are potential sources of information useful for solution structure determination of paramagnetic metalloproteins[37] which still have to be properly exploited. In this research, the nuclear relaxation enhancements are exploited as structural constraints after an appropriate theoretical analysis. Previously, a relationship was shown to be operative between the hyperfine shift of the β protons of the cysteines and the molar ratio of the two species having different valence distributions which are in equilibrium in solution.[7] Such a relationship was used in the present investigation to help in obtaining the solution structure of the protein.

At the end, an analysis of the electron relaxation properties of the cluster was possible.

IC970057V

(38) Mouesca, J. M.; Rius, G. J.; Lamotte, B. *J. Am. Chem. Soc.* **1993**, *115*, 4714−4731.
(39) Belinskii, M. I.; Bertini, I.; Galas, O.; Luchinat, C. *Inorg. Chim. Acta* **1996**, *243*, 91−99.
(40) Bertini, I.; Felli, I. C.; Luchinat, C.; Rosato, A. *Proteins: Struct., Funct., Genet.* **1996**, *24*, 158−164.
(41) Gochin, M.; Roder, H. *Protein Sci.* **1995**, *4*, 296−305.
(42) Banci, L.; Bertini, I.; Bren, K. L.; Cremonini, M. A.; Gray, H. B.; Luchinat, C.; Turano, P. *JBIC, J. Biol. Inorg. Chem.* **1996**, *1*, 117−126.
(43) Banci, L.; Bertini, I.; Gori Savellini, G.; Romagnoli, A.; Turano, P.; Cremonini, M. A.; Luchinat, C.; Gray, H. B. *Proteins: Struct., Funct., Genet.*, in press.
(44) Summers, M. F.; South, T. L.; Kim, B.; Hare, D. R. *Biochemistry* **1990**, *29*, 329−340.